Biomedical Signal Processing and Control 85 (2023) 104991

Contents lists available at ScienceDirect

Biomedical Signal Processing and Control

journal homepage: www.elsevier.com/locate/bspc

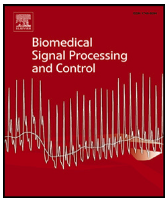

TripCEAiR: A multi-loss minimization approach for surface EMG based airwriting recognition☆

Ayush Tripathi [a], Prathosh A.P. [b], Suriya Prakash Muthukrishnan [c], Lalan Kumar [d,e,*]

[a] *Department of Electrical Engineering, Indian Institute of Technology Delhi, New Delhi, 110016, India*
[b] *Department of Electrical Communication Engineering, Indian Institute of Science, Bengaluru 560012, India*
[c] *Department of Physiology, All India Institute of Medical Sciences, New Delhi, 110016, India*
[d] *Bharti School of Telecommunication, Indian Institute of Technology Delhi, New Delhi, 110016, India*
[e] *Yardi School of Artificial Intelligence, Indian Institute of Technology Delhi, New Delhi, 110016, India*

ARTICLE INFO

Keywords:
Electromyography
Human computer interaction
Airwriting
Gesture recognition
Triplet loss
Muscle computer interface

ABSTRACT

Airwriting Recognition refers to the problem of identification of letters written in space with movement of the finger. It can be seen as a special case of dynamic gesture recognition wherein the set of gestures are letters in a particular language. Surface Electromyography (sEMG) is a non-invasive approach used to capture electrical signals generated as a result of contraction and relaxation of the muscles. sEMG has been widely adopted for gesture recognition applications. Unlike static gestures, dynamic gestures are user-friendly and can be used as a method for input with applications in Human Computer Interaction. There has been limited work in recognition of dynamic gestures such as airwriting, using sEMG signals and forms the core of the current work. In this work, a multi-loss minimization framework for sEMG based airwriting recognition is proposed. The proposed framework aims at learning a feature embedding vector that minimizes the triplet loss, while simultaneously learning the parameters of a classifier head to recognize corresponding alphabets. The proposed method is validated on a dataset recorded in the lab comprising of sEMG signals from 50 participants writing English uppercase alphabets. The effect of different variations of triplet loss, triplet mining strategies and feature embedding dimension is also presented. The best-achieved accuracy was 81.26% and 65.62% in user-dependent and independent scenarios respectively by using semihard positive and hard negative triplet mining. The code for our implementation will be made available at https://github.com/ayushayt/TripCEAiR

1. Introduction

1.1. Background

The ability to communicate is one of the most important of all life skills that humans possess. The rapid emergence of digital devices has led to a proportional increment in Human Computer Interaction (HCI). However, the medium of user input to HCI systems is limited to traditional methods such as touchscreen, keyboard, and mouse. Therefore, there is a growing demand of alternate HCI input modalities to reduce the need for such additional devices. In this regard, airwriting recognition seems to be a viable solution. Airwriting is referred to as the task of writing in space with the movement of the finger [1,2]. The unrestricted nature of free space writing provides the user with a seamless method to provide input for HCI applications. Additionally, since the gesture vocabulary is same as that of letters in a language, a user is not required to learn any new gestures for using such a system. Airwriting Recognition has been tackled by using different methods, such as wrist-worn Inertial Measurement Unit [3,4], smartphone [5], wearable glove [6], Wii remote [7], finger ring [8], and computer vision based methods [9]. In this work, a surface Electromyography (sEMG) based airwriting recognition framework is proposed. sEMG is a physiological signal recorded by placing electrodes on the skin over the target muscle [10]. Due to its user-friendly and non-invasive nature, sEMG has been widely used for tasks such as sign language recognition [11], user authentication [12], human machine interaction [13], and prosthetic control [14].

☆ This work was supported in part by Prime Minister's Research Fellowship, (PMRF), India, Ministry of Education (MoE), Government of India.
This work involved human subjects or animals in its research. Approval of all ethical and experimental procedures and protocols was granted by the Institute Ethics Committee, India, All India Institute of Medical Sciences, New Delhi, India with reference number IEC-267/01.04.2022,RP-55/2022.

* Corresponding author at: Yardi School of Artificial Intelligence, Indian Institute of Technology Delhi, New Delhi, 110016, India.
E-mail addresses: ayush.tripathi@ee.iitd.ac.in (A. Tripathi), prathosh@iisc.ac.in (P. A.P.), dr.suriyaprakash@aiims.edu (S.P. Muthukrishnan), lkumar@ee.iitd.ac.in (L. Kumar).

https://doi.org/10.1016/j.bspc.2023.104991
Received 2 January 2023; Received in revised form 22 March 2023; Accepted 30 April 2023
Available online 10 May 2023

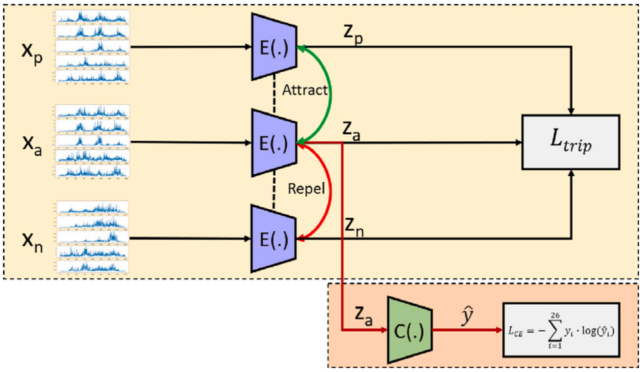

Fig. 1. Block diagram depicting the proposed method. Encoder and classifier blocks are represented by $E(\cdot)$ and $C(\cdot)$ respectively. The model parameters are optimized by minimizing L_{trip} and L_{CE} simultaneously in an end-to-end manner. The dashed lines indicate that the encoders have shared weights. x_a, x_p, and x_n denote the anchor, positive, and negative samples respectively.

1.2. *Related work*

Gesture recognition using sEMG signals has been used for several applications such as sign language recognition [15], user authentication [16], robot control [17], and rehabilitation [18]. The literature on sEMG based hand gesture recognition can be divided into either static or dynamic gesture recognition. The focus of static gesture recognition is to identify the gestures formed by specified hand shape with no temporal dimension. Several attempts including handcrafted features with machine learning [13], and deep learning [19] have been proposed for development of static gesture recognition systems. Additionally, several time-domain features [20,21], frequency-domain features [22] and image representations [23–25] of sEMG signals have also been utilized for solving the task of static gesture recognition. In case of dynamic gesture recognition, the task is to identify gestures formed by motion of the hand in space. This adds a temporal dimension to the gestures and thus it becomes essential to simultaneously consider the shape, position and movement of the hand for accurate prediction of the gesture. A CNN-based model trained on time-frequency images was proposed in [26] for identification of 5 dynamic hand gestures. In [27], the authors proposed a multi-stream residual network for 6-class dynamic hand gesture recognition system using sEMG signals. A specific use case of dynamic gesture recognition is the task of handwriting recognition, where the vocabulary of dynamic gestures is the alphabets in a language. A dynamic time warping based approach for handwriting recognition was proposed in [28], and further improved in [29]. A CNN–LSTM based framework for classifying 36 different gestures, which included 26 uppercase English alphabets and digits 0–9 was proposed in [30]. Unlike handwriting, the task of airwriting recognition is aimed at identifying characters written in free space, without any visual and haptic feedback during the process of writing. In literature, various airwriting recognition systems have been proposed by using inertial sensors [3,4,31] and computer vision based techniques [32,33]. However, there has been limited work in recognition of airwriting by using sEMG signals. To the best of the author's knowledge, an airwriting recognition based on sEMG signals was first proposed in [34]. Different time-domain features were utilized to construct sEMG envelopes along with time-frequency images to form input to several deep learning based models for the task of airwriting recognition on a dataset collected in the lab (SurfMyoAiR). Motivated by this, the current study explores a multi-loss minimization approach for airwriting recognition from sEMG signals obtained from a user's forearm muscles.

1.3. *Objectives and contributions*

In this work, a multi-loss minimization framework for sEMG based airwriting recognition is proposed. The central idea behind the approach is to simultaneously learn feature embeddings from sEMG signals and identify the character corresponding to the given input signal. An encoder block is used to extract embeddings from the input sEMG signal, the parameters of which are learnt by minimizing the triplet loss. The intuition behind triplet loss is to attract the embeddings of an anchor sample close to the embeddings of another sample from the same class (positive sample), while repelling it away from that of a different class (negative sample). These embedding vectors are simultaneously fed to a classifier head, the parameters of which are learnt by minimizing the cross entropy loss for classifying the embeddings into one of the 26 classes (corresponding to English uppercase alphabets). The entire model is trained in an end-to-end manner by minimizing the sum of triplet and cross entropy losses. The performance of the proposed algorithm is evaluated by performing both user-independent and user-dependent 5-fold validation on a dataset comprising of sEMG recordings from 50 participants while writing uppercase English alphabets, collected in the lab. The evaluation is performed by taking three different variants of the triplet loss. Additionally, the variation of recognition accuracies with respect to feature embedding dimension and the choice of triplet mining strategies has been comprehensively explored.

2. Methodology

The proposed TripCEAiR framework, depicted in Fig. 1 comprises of two sub-networks: an encoder and a classifier head. The encoder network is used to obtain the feature embeddings by minimizing the triplet loss. The embeddings are subsequently used as input to the classifier network, the parameters of which are learnt by cross-entropy loss minimization. The model is trained in an end-to-end fashion to learn the parameters of both the encoder and the classifier.

2.1. *Proposed framework*

The input to the model is a multivariate time series comprising of processed sEMG signals recorded while writing English uppercase alphabets. The sEMG signals are obtained from 5 different locations on the forearm, thereby resulting in a total of five time series per sample. A batch of size N is represented as $\{x_j, y_j\}_{j=1,2,..N}$, where $x_j \in \mathcal{X}$ is the input multivariate time series, and $y_j \in \{A, \ldots, Z\}$ is the corresponding alphabet label. The encoder network represented by $E(.) : \mathcal{X} \rightarrow \mathbb{R}^{|E|}$, is used to map the input x_j to an embedding vector z_j. The parameters of the encoder network denoted by θ_E, are learnt by minimizing the triplet loss (L_{trip}) over the embedding vectors after normalizing them to a unit hypersphere (represented by $\tilde{z_j}$). Minimizing the triplet loss aims at bringing the anchor embedding close to the corresponding positive embedding, while simultaneously pushing it away from the negative embedding. In particular, three different variations of triplet loss are utilized for learning the encoder parameters.

2.1.1. *N-pair based triplet loss*

A modification of the standard N-pair loss [35] is utilized for learning the feature embeddings. The loss aims at pulling the positive and anchor close to each other while repelling the anchor and negative embeddings by using dot product as a measure of similarity between the embedding vectors. Mathematically, it is given as,

$$L_{trip-NP} = \sum_{T(\tilde{z_a})} -log \frac{exp(\frac{\tilde{z_a} \cdot \tilde{z_p}}{\tau})}{exp(\frac{\tilde{z_a} \cdot \tilde{z_p}}{\tau}) + exp(\frac{\tilde{z_a} \cdot \tilde{z_n}}{\tau})} \tag{1}$$

where $T(\tilde{z_a})$ denotes the set of all possible triplets in a batch, τ is a scalar parameter (referred to as temperature) and $z_1 \cdot z_2$ represents the inner product between embedding vectors z_1 and z_2.

Table 1
Details of the proposed 1DCNN-BiLSTM based encoder.

Layer	Kernel size	# of filters	Layer parameters
BatchNorm	–	–	–
Conv1D	10	128	Stride = 1, Activation = ReLU, Zero padding
MaxPool1D	3		Strides = 3, No Padding
Conv1D	10	128	Stride = 1, Activation = ReLU, Zero padding
MaxPool1D	3		Strides = 3, No Padding
Conv1D	10	256	Stride = 1, Activation = ReLU, Zero padding
MaxPool1D	3		Strides = 3, No Padding
Conv1D	10	256	Stride = 1, Activation = ReLU, Zero padding
MaxPool1D	3		Strides = 3, No Padding
BiLSTM	–	–	Hidden states = 512, Activation = tanh
Dense	–	–	Neurons = $\|E\|$, Activation = ReLU

2.1.2. Margin based triplet loss with L^2 norm

The intuition behind this loss is to minimize the distance between the anchor and positive embeddings while maximizing the distance between the anchor and negative embeddings. Therefore, the objective is to learn embeddings such that, $\|\tilde{z}_a - \tilde{z}_n\|_2^2 \geq \|\tilde{z}_a - \tilde{z}_p\|_2^2 + \alpha$. Here, $\|\cdot\|_2^2$ denotes the square of L^2 norm and α is referred to as the margin parameter. To achieve this objective, the loss function is defined as,

$$L_{trip-L2} = \begin{cases} 0, & \text{if } d_{ap} + \alpha \leq d_{an} \\ d_{ap} - d_{an} + \alpha, & \text{otherwise} \end{cases} \tag{2}$$

In the equation above, $d_{ap} = \|\tilde{z}_a - \tilde{z}_p\|_2^2$, and $d_{an} = \|\tilde{z}_a - \tilde{z}_n\|_2^2$. By minimizing this loss function, the distance between embeddings of anchor and positive pairs is minimized only when it is greater than the distance between the corresponding anchor and negative pair by a factor α. For triplets where this margin is not violated, the loss is set to 0. More specifically, the current study uses a smooth version of the aforementioned loss, given by:

$$L_{trip-L2} = \sum_{T(\tilde{z}_a)} log[1 + exp\{d_{ap} - d_{an} + \alpha\}] \tag{3}$$

where, $T(\tilde{z}_a)$ represents the set of all possible triplets within a batch.

2.1.3. Margin based triplet loss with cosine similarity

Similar to the margin based loss with L^2 norm, the intuition behind this loss is to maximize the similarity between anchor and positive embeddings, while minimizing the similarity between anchor and negative embeddings. The similarity is measured using cosine distance as the metric. In particular, the embeddings are learnt such that $\tilde{z}_a \cdot \tilde{z}_p \geq \tilde{z}_a \cdot \tilde{z}_n + \alpha$. This objective is achieved by defining the loss function as,

$$L_{trip-CD} = \begin{cases} 0, & \text{if } s_{an} + \alpha \leq s_{ap} \\ s_{an} - s_{ap} + \alpha, & \text{otherwise} \end{cases} \tag{4}$$

where, $s_{ap} = \tilde{z}_a \cdot \tilde{z}_p$, and $s_{an} = \tilde{z}_a \cdot \tilde{z}_n$. The intuition behind this loss is similar to that of the margin based loss with L^2 norm, where the difference lies in the measure of similarity. With $T(\tilde{z}_a)$ representing the set of triplets in the batch, the smoothed loss function used in the current study is defined as,

$$L_{trip-CD} = \sum_{T(\tilde{z}_a)} log[1 + exp\{s_{an} - s_{ap} + \alpha\}] \tag{5}$$

The embeddings obtained as output of the encoder block (z_j) are simultaneously fed to a classifier network, $C(\cdot)$ which is a mapping from the embedding space to the set of alphabets. The output of the classifier is a 26 dimensional vector given by $\hat{y} = C(z) = \sigma(\theta_C^T z)$. Here, θ_C are the classifier parameters, which are learnt by minimizing the cross-entropy loss (L_{CE}) and $\sigma(\cdot)$ denotes the softmax activation function. The parameters of both encoder and classifier networks are learnt in an end-to-end fashion by minimizing the sum of the two individual losses. Therefore, the final loss to be minimized is the linear combination of the two losses

$$L = L_{trip} + L_{CE} \tag{6}$$

It is to be noted that the triplet loss does not add any additional parameters and hence, during inference, size of the model is same as that of a model trained by only minimizing the cross entropy loss.

2.2. Triplet mining strategies

Given a batch of N training samples with the input multivariate time series denoted by x and the corresponding label y_x, the embedding vector is computed as $z = E(x)$. For an anchor sample x_a (with embedding z_a), the corresponding positive and negative are denoted as x_p and x_n (with embeddings z_p and z_n) respectively. In this work, several positive and negative mining strategies for forming the triplets are explored [36,37]. These different strategies are detailed in the following subsections.

2.2.1. Easy positive mining

The sample x_{EP} within a batch, the embedding of which is closest to that of the anchor and belongs to the same class is referred to as an easy positive. Mathematically easy positive samples are identified as,

$$x_{EP} = \underset{x:y_x = y_{x_a}}{\operatorname{argmin}} \|z_a - z\|_2 \tag{7}$$

Easy positive mining pulls only the embeddings of two closest positives towards each other. This helps in reducing overclustering and improves generalization of embeddings.

2.2.2. Hard positive mining

Hard positives (x_{HP}) are the samples belonging to the same class as the anchor within the batch that have least similarity with the anchor embeddings.

$$x_{HP} = \underset{x:y_x = y_{x_a}}{\operatorname{argmax}} \|z_a - z\|_2 \tag{8}$$

Such a positive mining strategy leads to tight clustering of similar classes in the embedding space. This leads to a decrease in variance and may converge to local minima.

2.2.3. Semihard positive mining

Semihard positive mining aims to select the positive sample from the batch such that, in the embedding space, it is closer from the anchor than the selected negative sample (based on the negative mining strategy). Mathematically, it is represented as,

$$x_{SHP} = \underset{\substack{y_x = y_{x_a} \\ x:\|z_a - z\|_2 < \|z_a - z_n\|_2}}{\operatorname{argmax}} \|z_a - z\|_2 \tag{9}$$

Such a mining strategy mitigates the issues of convergence to local minima and possibility of a collapsed model as in case of hard positive mining, while still ensuring tight clustering of the samples belonging to the same class [37].

2.2.4. Negative mining

Analogous to the positive mining easy, hard, and semihard negatives correspond to samples selected from the batch that belong to a different class from the anchor. Mathematically, it is defined as,

$$x_{EN} = \underset{x:y_x \neq y_{x_a}}{\operatorname{argmax}} \|z_a - z\|_2 \tag{10}$$

$$x_{HN} = \underset{x:y_x \neq y_{x_a}}{\operatorname{argmin}} \|z_a - z\|_2 \tag{11}$$

$$x_{SHN} = \underset{\substack{y_x \neq y_{x_a} \\ x:\|z_a - z\|_2 > \|z_a - z_p\|_2}}{\operatorname{argmin}} \|z_a - z\|_2 \tag{12}$$

Theoretically, easy negatives correspond to the most dissimilar sample within the batch. Hard negative is the sample with the closest embedding to that of the anchor but has a different class label. Similarly, semihard negative chooses a negative from the batch in a way that the embeddings of anchor and the negative are farther than the embeddings of the anchor with the selected positive (based on the positive mining strategy).

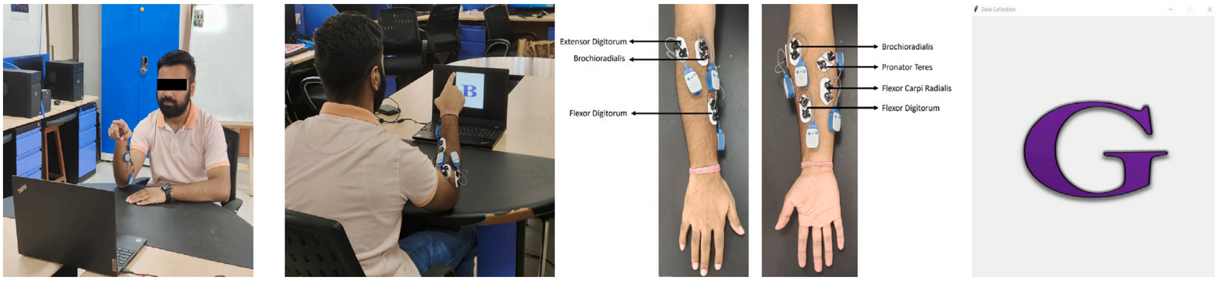
[redacted]

Fig. 2. Depiction of the sEMG signal recording setup, the electrode placement locations, and the visual stimulus presented to the participant.
Source: The figures have been adapted from [34].

Table 2
Recognition accuracies for the user-independent airwriting recognition task by using different triplet mining strategies and feature embedding dimension. Entries in blue denote best achieved accuracy for each embedding dimension and the best overall accuracy is depicted in bold.

Loss	Mining strategy		Embedding dimension				
	Positive	Negative	32	64	128	256	512
L_{CE}	–	–	0.6325	0.6345	0.6322	0.6278	0.6340
$L_{trip-NP} + L_{CE}$	Easy	Easy	0.6277	0.6417	0.6367	0.6409	0.6361
	Easy	Hard	0.6294	0.6376	0.6412	0.6490	0.6457
	Easy	Semihard	0.6394	0.6456	0.6492	0.6433	0.6462
	Easy	All	0.6339	0.6378	0.6445	0.6447	0.6411
	Hard	Easy	0.6298	0.6292	0.6358	0.6294	0.6302
	Hard	Hard	0.6083	0.6172	0.6195	0.6221	0.6188
	Hard	Semihard	0.6372	0.6465	0.6356	0.6432	0.6488
	Hard	All	0.6228	0.6164	0.6266	0.6301	0.6259
	Semihard	Easy	0.6306	0.6340	0.6363	0.6243	0.6295
	Semihard	Hard	0.6462	0.6483	0.6546	**0.6562**	0.6553
	All	Easy	0.6272	0.6348	0.6287	0.6354	0.6347
	All	Hard	0.6095	0.6365	0.6383	0.6331	0.6375
	All	All	0.6423	0.6342	0.6394	0.6422	0.6466
$L_{trip-CD} + L_{CE}$	Easy	Easy	0.6048	0.6226	0.6286	0.6263	0.6175
	Easy	Hard	0.6393	0.6355	0.6323	0.6307	0.6314
	Easy	Semihard	0.6358	0.6388	0.6354	0.6355	0.6295
	Easy	All	0.6233	0.6280	0.6313	0.6387	0.6405
	Hard	Easy	0.6066	0.6155	0.6251	0.6223	0.6202
	Hard	Hard	0.6248	0.6176	0.6219	0.6272	0.6246
	Hard	Semihard	0.6282	0.6336	0.6317	0.6369	0.6332
	Hard	All	0.6267	0.6308	0.6356	0.6376	0.6327
	Semihard	Easy	0.6022	0.6158	0.6227	0.6245	0.6151
	Semihard	Hard	0.6305	0.6351	0.6328	0.6244	0.6372
	All	Easy	0.6092	0.6302	0.6255	0.6287	0.6262
	All	Hard	0.6307	0.6225	0.6310	0.6412	0.6279
	All	All	0.6308	0.6403	0.6420	0.6417	0.6355
$L_{trip-L2} + L_{CE}$	Easy	Easy	0.6236	0.6222	0.6328	0.6298	0.6251
	Easy	Hard	0.6241	0.6328	0.6333	0.6415	0.6393
	Easy	Semihard	0.6412	0.6392	0.6388	0.6286	0.6261
	Easy	All	0.6410	0.6399	0.6391	0.6431	0.6397
	Hard	Easy	0.6158	0.6272	0.6217	0.6261	0.6210
	Hard	Hard	0.6126	0.6285	0.6198	0.6314	0.6273
	Hard	Semihard	0.6327	0.6431	0.6364	0.6362	0.6412
	Hard	All	0.6211	0.6358	0.6347	0.6359	0.6377
	Semihard	Easy	0.6125	0.6193	0.6252	0.6145	0.6169
	Semihard	Hard	0.6424	0.6394	0.6495	0.6402	0.6367
	All	Easy	0.6262	0.6179	0.6307	0.6218	0.6275
	All	Hard	0.6112	0.6395	0.6356	0.6273	0.6332
	All	All	0.6292	0.6420	0.6437	0.6412	0.6419

Table 3
Recognition accuracies for the user-dependent airwriting recognition task by using different triplet mining strategies and feature embedding dimension. Entries in blue denote best achieved accuracy for each embedding dimension and the best overall accuracy is depicted in bold.

Loss	Mining strategy		Embedding dimension				
	Positive	Negative	32	64	128	256	512
L_{CE}	–	–	0.7549	0.7712	0.7748	0.7725	0.7701
$L_{trip-NP} + L_{CE}$	Easy	Easy	0.7583	0.7664	0.7823	0.7764	0.7815
	Easy	Hard	0.7725	0.7792	0.7840	0.7898	0.7924
	Easy	Semihard	0.7867	0.7999	0.7955	0.7898	0.7904
	Easy	All	0.7781	0.7761	0.7729	0.7900	0.7856
	Hard	Easy	0.7484	0.7677	0.7665	0.7772	0.7718
	Hard	Hard	0.7533	0.7445	0.7684	0.7677	0.7645
	Hard	Semihard	0.7836	0.7843	0.7906	0.7852	0.7992
	Hard	All	0.7608	0.7829	0.7879	0.7778	0.7744
	Semihard	Easy	0.7555	0.7611	0.7677	0.7705	0.7745
	Semihard	Hard	0.7861	0.8035	0.8053	**0.8126**	0.8089
	All	Easy	0.7545	0.7575	0.7641	0.7811	0.7797
	All	Hard	0.7709	0.7701	0.7819	0.7540	0.7533
	All	All	0.7826	0.7879	0.7938	0.7847	0.7872
$L_{trip-CD} + L_{CE}$	Easy	Easy	0.7379	0.7505	0.7548	0.7606	0.7620
	Easy	Hard	0.7518	0.7688	0.7742	0.7746	0.7657
	Easy	Semihard	0.7606	0.7715	0.7675	0.7782	0.7547
	Easy	All	0.7557	0.7667	0.7795	0.7882	0.7815
	Hard	Easy	0.7334	0.7571	0.7628	0.7509	0.7335
	Hard	Hard	0.7558	0.7500	0.7749	0.7645	0.7717
	Hard	Semihard	0.7565	0.7751	0.7655	0.7766	0.7718
	Hard	All	0.7606	0.7698	0.7724	0.7794	0.7668
	Semihard	Easy	0.7482	0.7413	0.7545	0.7513	0.7325
	Semihard	Hard	0.7843	0.7678	0.7821	0.7788	0.7712
	All	Easy	0.7428	0.7552	0.7603	0.7680	0.7660
	All	Hard	0.7610	0.7484	0.7489	0.7675	0.7685
	All	All	0.7650	0.7893	0.7822	0.7772	0.7922
$L_{trip-L2} + L_{CE}$	Easy	Easy	0.7466	0.7656	0.7673	0.7622	0.7645
	Easy	Hard	0.7718	0.7689	0.7724	0.7782	0.7723
	Easy	Semihard	0.7697	0.7743	0.7565	0.7874	0.7658
	Easy	All	0.7550	0.7725	0.7838	0.7887	0.7908
	Hard	Easy	0.7512	0.7580	0.7688	0.7665	0.7568
	Hard	Hard	0.7422	0.7672	0.7659	0.7488	0.7408
	Hard	Semihard	0.7692	0.7778	0.7769	0.7808	0.7952
	Hard	All	0.7500	0.7722	0.7810	0.7815	0.7702
	Semihard	Easy	0.7356	0.7498	0.7572	0.7587	0.7672
	Semihard	Hard	0.7891	0.7778	0.7929	0.7871	0.7906
	All	Easy	0.7489	0.7572	0.7608	0.7725	0.7622
	All	Hard	0.7575	0.7604	0.7652	0.7682	0.7659
	All	All	0.7682	0.7896	0.7925	0.7892	0.7894

2.3. Model architecture

For the encoder block, an architecture based on a combination of Convolutional Neural Network (CNN) and Bidirectional Long Short Term Memory (BiLSTM) is used. The intuition behind selecting this particular architecture is that the convolutional layers extract the spatial features from the processed sEMG signals. The BiLSTM layer then aims at learning the temporal dimension from these spatial features. The details of the encoder architecture are presented in Table 1. First, Batch Normalization is applied to the processed signals, which are further passed through 4 convolutional layers each with a kernel size of 10. For the first couple of convolution layers, the numbers of kernels is set to 128, while it is increased to 256 for the last two layers. Maxpooling with a pool size of 3 is performed after each convolution layer. The features are then fed to a BiLSTM layer with 512 units. Rectified Linear Unit ($ReLU$) activation function is used for all the convolution layers and hyperbolic tangent ($tanh$) for the BiLSTM layer. The output of the 1DCNN-BiLSTM is subsequently fed to a dense layer comprising of

Table 4
Alphabet-wise precision, recall and F1-score corresponding to Semihard positive and Hard negative mining with $L_{trip-NP}+L_{CE}$ loss in user-independent, and user-dependent evaluation settings.

Alphabet	User independent			User dependent		
	Precision	Recall	F1-Score	Precision	Recall	F1-Score
A	0.73	0.74	0.74	0.87	0.84	0.86
B	0.74	0.69	0.72	0.88	0.84	0.86
C	0.69	0.73	0.71	0.77	0.78	0.77
D	0.54	0.51	0.52	0.68	0.67	0.67
E	0.68	0.74	0.71	0.84	0.83	0.83
F	0.65	0.62	0.63	0.79	0.80	0.80
G	0.70	0.66	0.68	0.84	0.82	0.83
H	0.69	0.67	0.68	0.84	0.82	0.83
I	0.59	0.52	0.55	0.81	0.75	0.78
J	0.64	0.59	0.61	0.82	0.82	0.82
K	0.66	0.65	0.65	0.81	0.77	0.79
L	0.64	0.69	0.66	0.81	0.80	0.81
M	0.74	0.76	0.75	0.87	0.90	0.88
N	0.59	0.61	0.60	0.77	0.77	0.77
O	0.67	0.66	0.67	0.79	0.78	0.79
P	0.57	0.56	0.56	0.71	0.70	0.71
Q	0.65	0.63	0.64	0.82	0.83	0.83
R	0.64	0.64	0.64	0.76	0.82	0.79
S	0.73	0.81	0.77	0.85	0.87	0.86
T	0.56	0.55	0.56	0.78	0.78	0.78
U	0.64	0.64	0.64	0.71	0.77	0.74
V	0.64	0.69	0.67	0.79	0.80	0.79
W	0.67	0.72	0.69	0.81	0.82	0.82
X	0.65	0.68	0.66	0.82	0.84	0.83
Y	0.64	0.62	0.63	0.85	0.79	0.82
Z	0.73	0.71	0.72	0.82	0.85	0.84

$|E|$ neurons and activated by ReLU activation function to obtain the embedding vector. Further, the classifier head is taken to be a single fully-connected layer having 26 neurons. A dropout of 50% is used in order to avoid overfitting.

3. Experiments and results

3.1. Dataset description

The recording of sEMG signals was done as per guidelines laid down in the Helsinki Declaration, and was ethically approved by the Institute Ethics Committee of the All India Institute of Medical Sciences, New Delhi. The dataset comprises of sEMG signals recorded from five forearm muscles (Flexor Carpi Radialis, Pronator teres, Flexor Digitorum, Brachioradialis, and Extensor Digitorum) while writing English uppercase alphabets (10 times). A total of 50 healthy subjects with mean age of 23.12 years participated in the experiment with written consent. In order to record the sEMG signals, Noraxon Ultium wireless sEMG sensor [38] and gel-based, self-adhesive Ag/AgCl disposable dual electrodes were used. The sEMG signals were recorded at a sampling rate of 2 kHz. During the processing stage, the recorded signals were downsampled to 500 Hz and absolute value of the signals was retained. A user interface operated by the experimenter was used to provide visual cue to the participant for the alphabet to be written. Random shuffling of alphabets within a set was done and the participant was provided adequate rest after 2 repetitions of the alphabet set. The data collection setup, location of sEMG electrodes on the forearm, and a sample visual stimulus are presented in Fig. 2.

3.2. Experimental details

The recorded sEMG signals correspond to different letters from different users, thereby leading to a variation in the length of signals. To mitigate this, the absolute sEMG signals are interpolated to a length of L samples using cubic interpolation if the signal was shorter and the extra samples were discarded, otherwise. The length L was taken to be 2000 samples which corresponds to 4 s duration of writing. Subsequently, z-normalization was performed to each of the processed signals individually.

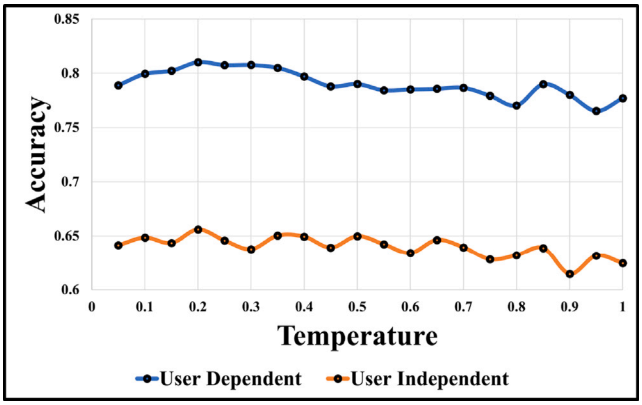

Fig. 3. Effect of temperature parameter on recognition accuracy for sEMG based airwriting recognition in user dependent and independent scenarios.

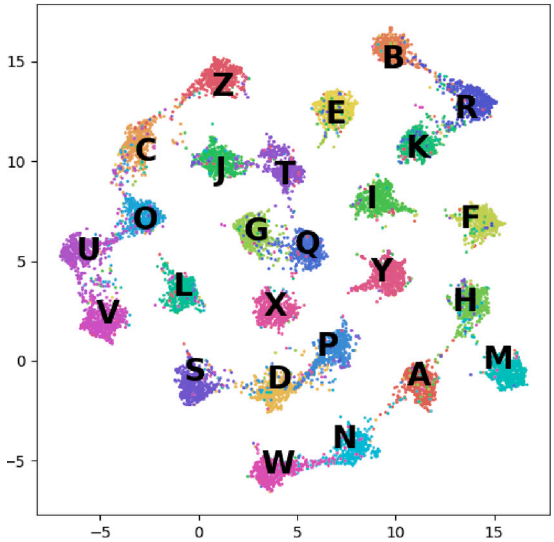

Fig. 4. Scatter plot depicting clusters for the different alphabets in the embedding space.

In order to check for robustness of the proposed method, experiments were performed in both user-independent and user-dependent settings. In the user-independent approach, 5-fold validation was performed while ensuring no subject overlap in the training and test sets. More specifically, in each fold, data corresponding to 40 subjects was used for training the model and evaluation was performed on the held-out subjects. Similarly, in the user-dependent setting, 5-fold validation was performed by splitting the entire data based on the repetition number during the airwriting data collection process. In each fold, the model was trained on 8 repetitions of all the subjects, and tested on the left out 2 repetitions. The training data was further split in an 80 : 20 ratio to form the training and validation sets. A mini-batch training process with a batch size of 260 was employed and the parameters of the model were updated using the Adam optimizer. Early stopping with a patience of 10 epochs while monitoring the validation accuracy was employed to avoid overfitting of the model.

3.3. Results and discussion

The effect of variation in mean recognition accuracies with different values of the temperature parameter (τ) for the N-pair based triplet

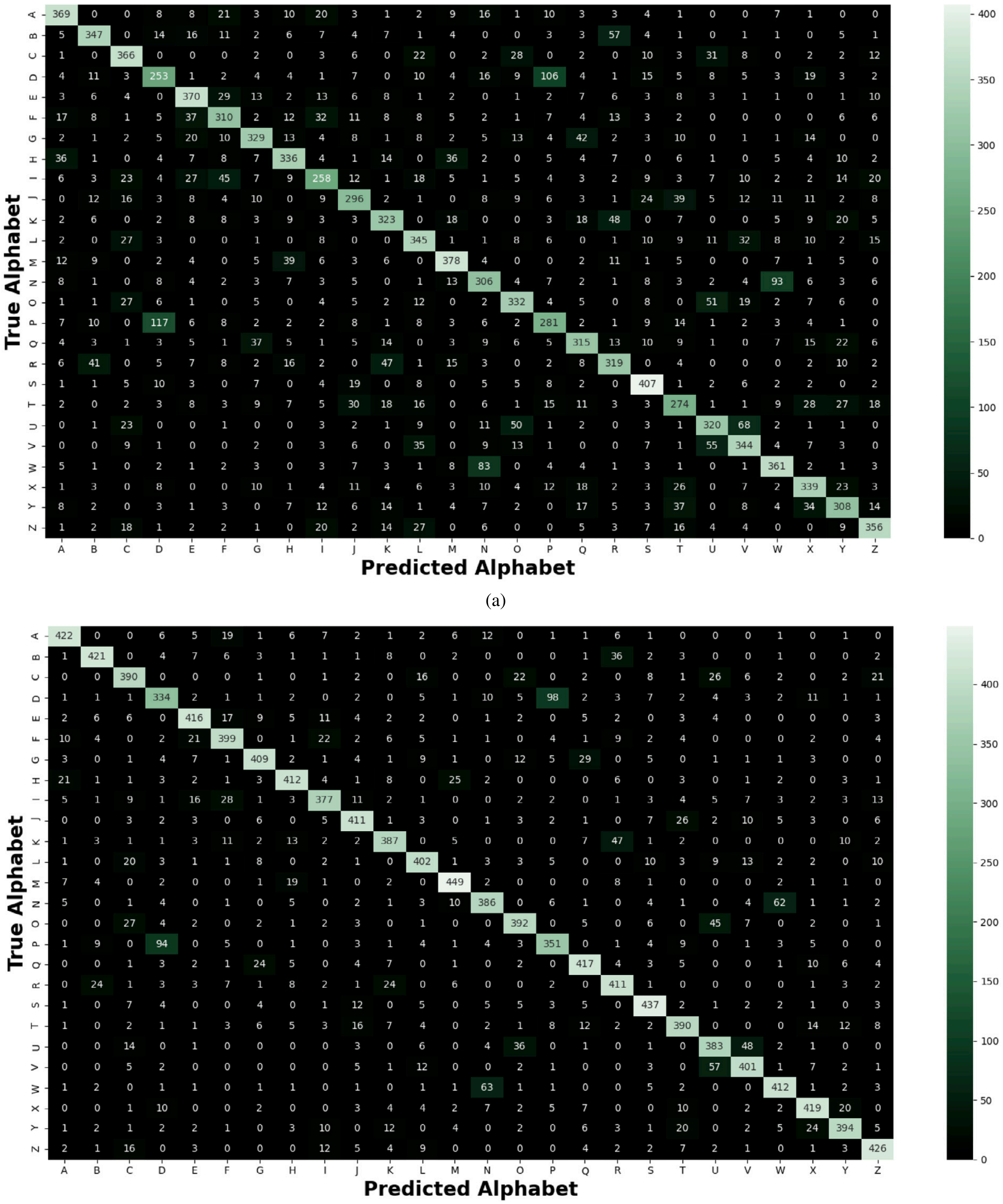

(a)

(b)

Fig. 5. Confusion matrices corresponding to Semihard positive and Hard negative mining with $L_{trip-NP} + L_{CE}$ loss in (a) user-independent, and (b) user-dependent evaluation settings.

loss are presented in Fig. 3. For observing the role of τ, the embedding dimension is set to 256, along with semihard positive and hard triplet mining. It is observed that the best accuracy is achieved with $\tau = 0.2$, and this value is retained for all subsequent experiments. Similarly, the optimal values of the margin parameter (α) in case of margin-based triplet loss is identified. The value is found to be $\alpha = 0.2$ and $\alpha = 0.1$ for margin loss with L^2 norm and cosine similarity, respectively. Tables 2 and 3 list the performance of the proposed architecture with the accuracies averaged across the 5 folds. The variation of accuracy with different feature embedding dimension (i.e. $|E|$), triplet mining strategies and the three variations of the triplet loss used in the study is also presented. It is observed from the tables that using the N-pair based triplet loss yields an improved accuracy compared to the margin based losses. It is seen that the best accuracy is achieved by using a feature embedding dimension of 256 along with semihard positive and hard negative mining. The superior accuracies obtained by using this triplet mining technique may be attributed to the fact that such a strategy pushes apart the most dissimilar samples while pulling those samples

Table 5
Comparison of different model architectures for sEMG based airwriting recognition task.

	Architecture	L_{CE}	$L_{trip-NP} + L_{CE}$	$L_{trip-L2} + L_{CE}$	$L_{trip-CD} + L_{CE}$
User dependent	1DCNN	0.6479	0.6522	0.6538	0.6506
	Stacked LSTM	0.4651	0.4419	0.4383	0.4400
	Stacked BiLSTM	0.4810	0.4545	0.4394	0.4479
	1DCNN-LSTM	0.7822	0.8089	0.7823	0.7746
	1DCNN-BiLSTM	0.7725	**0.8126**	0.7871	0.7788
User independent	1DCNN	0.5415	0.5432	0.5482	0.5552
	Stacked LSTM	0.3335	0.3221	0.3049	0.3103
	Stacked BiLSTM	0.4047	0.3692	0.3475	0.3419
	1DCNN-LSTM	0.6385	0.6559	0.6420	0.6375
	1DCNN-BiLSTM	0.6278	**0.6562**	0.6402	0.6244

Table 6
Details of the 1DCNN based encoder.

Layer	Kernel size	# of filters	Layer parameters
BatchNorm	–	–	–
Conv1D	10	128	Stride = 1, Activation = ReLU, Zero padding
MaxPool1D	3		Strides = 3, No Padding
Conv1D	10	128	Stride = 1, Activation = ReLU, Zero padding
MaxPool1D	3		Strides = 3, No Padding
Conv1D	10	256	Stride = 1, Activation = ReLU, Zero padding
MaxPool1D	3		Strides = 3, No Padding
Conv1D	10	256	Stride = 1, Activation = ReLU, Zero padding
MaxPool1D	3		Strides = 3, No Padding
GlobalAvgPool1D	–	–	–
Dense	–	–	Neurons = $\|E\|$, Activation = ReLU

Table 7
Details of the Stacked LSTM-based encoder.

Layer	Kernel size	# of filters	Layer parameters
BatchNorm	–	–	–
LSTM	–	–	Hidden states = 512, Activation = tanh
LSTM	–	–	Hidden states = 512, Activation = tanh
Dense	–	–	Neurons = $\|E\|$, Activation = ReLU

Table 8
Details of the Stacked Bidirectional LSTM-based encoder.

Layer	Kernel size	# of filters	Layer parameters
BatchNorm	–	–	–
BiLSTM	–	–	Hidden states = 512, Activation = tanh
BiLSTM	–	–	Hidden states = 512, Activation = tanh
Dense	–	–	Neurons = $\|E\|$, Activation = ReLU

Table 9
Details of the 1DCNN-LSTM based encoder.

Layer	Kernel size	# of filters	Layer parameters
BatchNorm	–		–
Conv1D	10	128	Stride = 1, Activation = ReLU, Zero padding
MaxPool1D	3		Strides = 3, No Padding
Conv1D	10	128	Stride = 1, Activation = ReLU, Zero padding
MaxPool1D	3		Strides = 3, No Padding
Conv1D	10	256	Stride = 1, Activation = ReLU, Zero padding
MaxPool1D	3		Strides = 3, No Padding
Conv1D	10	256	Stride = 1, Activation = ReLU, Zero padding
MaxPool1D	3		Strides = 3, No Padding
LSTM	–	–	Hidden states = 512, Activation = tanh
Dense	–	–	Neurons = $\|E\|$, Activation = ReLU

that are closer to the anchor than the hardest negative. The feature embedding vectors, which are the output of the encoder block (denoted by z) are visualized by reducing to 2 dimensions by using Uniform Manifold Approximation and Projection (UMAP). The plot depicting this visualization is presented in Fig. 4. The plot reveals tight clusters corresponding to each of the 26 uppercase English alphabets, with similar-looking alphabets (such as D & P) close to each other in the embedding space. The same is also observed from the confusion matrices presented in Fig. 5. It can be seen that similar-looking alphabets which are close to each other in the embedding space lead to the highest misclassification. Additionally, the precision, recall and F1-scores for individual alphabets is presented in Table 4. Overall, on combining the N-pair based triplet loss, an absolute improvement of 2.84% and 4.01% is observed in case of user independent and dependent scenarios respectively. Furthermore, the performance of the airwriting recognition system by using different model architectures including 1DCNN, Stacked Long Short Term Memory (LSTM), Bidirectional LSTM and 1DCNN-LSTM/BiLSTM is also presented in Table 5. The different encoder architectures used for this comparison are detailed in Tables 6–9 in Appendix. It is observed that the proposed 1DCNN-BiLSTM outperforms the other model architectures. This is attributed to the fact that in this architecture, the CNN layers act as a feature extractor and max pooling layer takes the average of the feature within a sliding window. The BiLSTM layer then learns the temporal characteristics from the extracted features. Hence, this combination of CNN-BiLSTM is able to better capture the nuances of the sEMG signal corresponding to different alphabets leading to superior performance.

4. Conclusion

In this paper, a multi-loss framework by combining triplet and cross entropy losses (TripCEAiR) for sEMG based airwriting recognition is proposed. Additionally, the effect of different triplet mining strategies and feature embedding dimension is comprehensively explored. It is seen that the proposed method outperforms the approach wherein model parameters are learnt by minimizing only the cross-entropy loss. An accuracy of 81.26% and 65.62% was obtained in the user-dependent and user-independent scenarios respectively by using semihard positive and hard negative mining and the N-pair based triplet loss. This implies an absolute improvement of 4.01% and 2.84% in the user-dependent and independent settings over the case when only cross-entropy loss is minimized. The improvement in recognition accuracies indicate the usability of the proposed framework in developing an sEMG based airwriting recognition system for HCI applications. Future work may be focused on exploring the robustness of the proposed sEMG based airwriting recognition system in adverse scenarios such as the presence of excessive noise and imperfect sensor placement.

CRediT authorship contribution statement

Ayush Tripathi: Conceptualization, Methodology, Data curation, Software, Formal analysis, Writing – original draft. **Prathosh A.P.:** Conceptualization, Methodology, Supervision, Formal analysis, Writing – review & editing. **Suriya Prakash Muthukrishnan:** Data Curation, Writing – review & editing. **Lalan Kumar:** Conceptualization, Methodology, Supervision, Writing – review & editing.

Declaration of competing interest

The authors declare that they have no known competing financial interests or personal relationships that could have appeared to influence the work reported in this paper.

Data availability

Data will be made available on request.

Appendix

Details of the encoder architectures used for comparison are presented in Tables 6–9.

References

[1] M. Chen, G. AlRegib, B.-H. Juang, Air-writing recognition—Part I: Modeling and recognition of characters, words, and connecting motions, IEEE Trans. Hum.-Mach. Syst. 46 (3) (2016) 403–413.

[2] M. Chen, G. AlRegib, B.-H. Juang, Air-writing recognition—Part II: Detection and recognition of writing activity in continuous stream of motion data, IEEE Trans. Hum.-Mach. Syst. 46 (3) (2016) 436–444.

[3] A. Tripathi, A.K. Mondal, L. Kumar, A.P. Prathosh, SCLAiR: Supervised contrastive learning for user and device independent airwriting recognition, IEEE Sens. Lett. 6 (2) (2022) 1–4.

[4] A. Tripathi, A.K. Mondal, L. Kumar, A.P. Prathosh, ImAiR: Airwriting recognition framework using image representation of IMU signals, IEEE Sens. Lett. 6 (10) (2022) 1–4.

[5] C. Li, C. Xie, B. Zhang, C. Chen, J. Han, Deep Fisher discriminant learning for mobile hand gesture recognition, Pattern Recognit. 77 (2018) 276–288.

[6] C. Amma, T. Schultz, Airwriting: Bringing text entry to wearable computers, XRDS: Crossroads ACM Mag. Stud. 20 (2) (2013) 50–55.

[7] S. Xu, Y. Xue, Air-writing characters modelling and recognition on modified CHMM, in: 2016 IEEE International Conference on Systems, Man, and Cybernetics, SMC, IEEE, 2016, pp. 001510–001513.

[8] L. Jing, Z. Dai, Y. Zhou, Wearable handwriting recognition with an inertial sensor on a finger nail, in: 2017 14th IAPR International Conference on Document Analysis and Recognition, Vol. 1, ICDAR, IEEE, 2017, pp. 1330–1337.

[9] A. Choudhury, K.K. Sarma, A CNN-LSTM based ensemble framework for in-air handwritten assamese character recognition, Multimedia Tools Appl. 80 (28) (2021) 35649–35684.

[10] V. Gohel, N. Mehendale, Review on electromyography signal acquisition and processing, Biophys. Rev. 12 (6) (2020) 1361–1367.

[11] T. Fouts, A. Hindy, C. Tanner, Sensors to sign language: A natural approach to equitable communication, in: ICASSP 2022 - 2022 IEEE International Conference on Acoustics, Speech and Signal Processing, ICASSP, 2022, pp. 8462–8466.

[12] X. Jiang, K. Xu, X. Liu, C. Dai, D.A. Clifton, E.A. Clancy, M. Akay, W. Chen, Neuromuscular password-based user authentication, IEEE Trans. Ind. Inform. 17 (4) (2021) 2641–2652.

[13] M. Simão, N. Mendes, O. Gibaru, P. Neto, A review on electromyography decoding and pattern recognition for human-machine interaction, IEEE Access 7 (2019) 39564–39582.

[14] O.W. Samuel, H. Zhou, X. Li, H. Wang, H. Zhang, A.K. Sangaiah, G. Li, Pattern recognition of electromyography signals based on novel time domain features for amputees' limb motion classification, Comput. Electr. Eng. 67 (2018) 646–655.

[15] S. Tateno, H. Liu, J. Ou, Development of sign language motion recognition system for hearing-impaired people using electromyography signal, Sensors 20 (20) (2020) 5807.

[16] Q. Li, Z. Luo, J. Zheng, A new deep anomaly detection-based method for user authentication using multichannel surface EMG signals of hand gestures, IEEE Trans. Instrum. Meas. 71 (2022) 1–11.

[17] B. Boru, K. Erin, Novel technique for control of industrial robots with wearable and contactless technologies, Measurement 192 (2022) 110850.

[18] H. Zhou, Q. Zhang, M. Zhang, S. Shahnewaz, S. Wei, J. Ruan, X. Zhang, L. Zhang, Toward hand pattern recognition in assistive and rehabilitation robotics using EMG and kinematics, Front. Neurorobot. 15 (2021) 50.

[19] W. Li, P. Shi, H. Yu, Gesture recognition using surface electromyography and deep learning for prostheses hand: state-of-the-art, challenges, and future, Front. Neurosci. 15 (2021) 621885.

[20] A.A. Neacsu, G. Cioroiu, A. Radoi, C. Burileanu, Automatic EMG-based hand gesture recognition system using time-domain descriptors and fully-connected neural networks, in: 2019 42nd International Conference on Telecommunications and Signal Processing, TSP, 2019, pp. 232–235.

[21] F. Duan, X. Ren, Y. Yang, A gesture recognition system based on time domain features and linear discriminant analysis, IEEE Trans. Cogn. Dev. Syst. 13 (1) (2021) 200–208.

[22] U. Côté Allard, F. Nougarou, C.L. Fall, P. Giguère, C. Gosselin, F. Laviolette, B. Gosselin, A convolutional neural network for robotic arm guidance using sEMG based frequency-features, in: 2016 IEEE/RSJ International Conference on Intelligent Robots and Systems, IROS, 2016, pp. 2464–2470.

[23] U. Côté-Allard, C.L. Fall, A. Drouin, A. Campeau-Lecours, C. Gosselin, K. Glette, F. Laviolette, B. Gosselin, Deep learning for electromyographic hand gesture signal classification using transfer learning, IEEE Trans. Neural Syst. Rehabil. Eng. 27 (4) (2019) 760–771.

[24] D.-C. Oh, Y.-U. Jo, Classification of hand gestures based on multi-channel EMG by scale average wavelet transform and convolutional neural network, Int. J. Control Autom. Syst. 19 (3) (2021) 1443–1450.

[25] M.A. Ozdemir, D.H. Kisa, O. Guren, A. Akan, Hand gesture classification using time–frequency images and transfer learning based on CNN, Biomed. Signal Process. Control 77 (2022) 103787.

[26] S. Song, L. Yang, M. Wu, Y. Liu, H. Yu, Dynamic hand gesture recognition via electromyographic signal based on convolutional neural network, in: 2021 IEEE International Conference on Systems, Man, and Cybernetics, SMC, 2021, pp. 876–881.

[27] Z. Yang, D. Jiang, Y. Sun, B. Tao, X. Tong, G. Jiang, M. Xu, J. Yun, Y. Liu, B. Chen, et al., Dynamic gesture recognition using surface EMG signals based on multi-stream residual network, Front. Bioeng. Biotechnol. 9 (2021).

[28] G. Huang, D. Zhang, X. Zheng, X. Zhu, An EMG-based handwriting recognition through dynamic time warping, in: 2010 Annual International Conference of the IEEE Engineering in Medicine and Biology, 2010, pp. 4902–4905.

[29] C. Li, Z. Ma, L. Yao, D. Zhang, Improvements on EMG-based handwriting recognition with DTW algorithm, in: 2013 35th Annual International Conference of the IEEE Engineering in Medicine and Biology Society, EMBC, IEEE, 2013, pp. 2144–2147.

[30] J.G. Beltran-Hernandez, J. Ruiz-Pinales, P. Lopez-Rodriguez, J.L. Lopez-Ramirez, J.G. Avina-Cervantes, Multi-stroke handwriting character recognition based on sEMG using convolutional-recurrent neural networks, Math. Biosci. Eng. 17 (5) (2020) 5432–5448.

[31] T. Yanay, E. Shmueli, Air-writing recognition using smart-bands, Pervasive Mob. Comput. 66 (2020) 101183.

[32] U.-H. Kim, Y. Hwang, S.-K. Lee, J.-H. Kim, Writing in the air: Unconstrained text recognition from finger movement using spatio-temporal convolution, 2021, arXiv preprint arXiv:2104.09021.

[33] S. Mukherjee, S.A. Ahmed, D.P. Dogra, S. Kar, P.P. Roy, Fingertip detection and tracking for recognition of air-writing in videos, Expert Syst. Appl. 136 (2019) 217–229.

[34] A. Tripathi, L. Kumar, A.P. Prathosh, S.P. Muthukrishnan, SurfMyoAiR: A surface electromyography based framework for airwriting recognition, 2022, arXiv preprint arXiv:2210.17185.

[35] K. Sohn, Improved deep metric learning with multi-class n-pair loss objective, Adv. Neural Inf. Process. Syst. 29 (2016).

[36] H. Xuan, A. Stylianou, R. Pless, Improved embeddings with easy positive triplet mining, in: 2020 IEEE Winter Conference on Applications of Computer Vision, WACV, 2020, pp. 2463–2471.

[37] F. Schroff, D. Kalenichenko, J. Philbin, FaceNet: A unified embedding for face recognition and clustering, in: 2015 IEEE Conference on Computer Vision and Pattern Recognition, CVPR, 2015, pp. 815–823.

[38] Noraxon Ultium EMG. https://www.noraxon.com/our-products/ultium-emg/.